polymers

MDPI

Article

Xanthate-Modified Magnetic Fe_3O_4@SiO_2-Based Polyvinyl Alcohol/Chitosan Composite Material for Efficient Removal of Heavy Metal Ions from Water

Shifan Wang [1], Yuan Liu [1], Aiwen Yang [1], Qi Zhu [1], Hua Sun [1], Po Sun [2], Bing Yao [1], Yunxiao Zang [1], Xihua Du [1] and Liming Dong [1,*]

[1] School of Material and Chemistry Engineering, Xuzhou University of Technology, Xuzhou 221018, China; shifanwang@xzit.edu.cn (S.W.); ly17305187957@163.com (Y.L.); yaw8023wbh@163.com (A.Y.); zq010214@163.com (Q.Z.); iamsunhua@xzit.edu.cn (H.S.); yaoming@xzit.edu.cn (B.Y.); yxzang@zxit.edu.cn (Y.Z.); dxh@xzit.edu.cn (X.D.)

[2] Analysis and Testing Central Facility, Anhui University of Technology, Maanshan 243032, China; sunpoo@ahut.edu.cn

* Correspondence: polymerdlm@163.com

Abstract: Chitosan has several shortcomings that limit its practical application for the adsorption of heavy metals: mechanical instability, a challenging separation and recovery process, and low equilibrium capacity. This study describes the synthesis of a magnetic xanthate-modified polyvinyl alcohol and chitosan composite (XMPC) for the efficient removal and recovery of heavy metal ions from aqueous solutions. The XMPC was synthesized from polyvinyl alcohol, chitosan, and magnetic Fe_3O_4@SiO_2 nanoparticles. The XMPC was characterized, and its adsorption performance in removing heavy metal ions was studied under different experimental conditions. The adsorption kinetics fit a pseudo-second-order kinetic model well. This showed that the adsorption of heavy metal ions by the XMPC is a chemical adsorption and is affected by intra-particle diffusion. The equilibrium adsorption isotherm was well described by the Langmuir and Freundlich equations. The XMPC reached adsorption equilibrium at 303 K after approximately 120 min, and the removal rate of Cd(II) ions was 307 mg/g. The composite material can be reused many times and is easily magnetically separated from the solution. This makes the XMPC a promising candidate for widespread application in sewage treatment systems for the removal of heavy metals.

Keywords: magnetic materials; chitosan; adsorption; heavy metal; modification

Citation: Wang, S.; Liu, Y.; Yang, A.; Zhu, Q.; Sun, H.; Sun, P.; Yao, B.; Zang, Y.; Du, X.; Dong, L. Xanthate-Modified Magnetic Fe_3O_4@SiO_2-Based Polyvinyl Alcohol/Chitosan Composite Material for Efficient Removal of Heavy Metal Ions from Water. *Polymers* **2022**, *14*, 1107. https://doi.org/10.3390/polym14061107

Academic Editor: Moonis Ali Khan

Received: 21 January 2022
Accepted: 3 March 2022
Published: 10 March 2022

1. Introduction

As the global population increases and the world becomes more industrialized, water pollution has become a rapidly escalating global environmental problem that threatens the lives of the planet's inhabitants. Water pollution originates from a variety of sources, and the availability of safe drinking water is of global concern, with the number of detected pollutants increasing, including inorganic anions, dyes, oil spills, and heavy metals. Heavy metals enter the environment from various sources, such as combustion, wastewater discharge, and production sites [1–3]. Heavy metal ions are water soluble and non-biodegradable and have many environmental, economic, and public health impacts [4,5]. Heavy metals are metals with densities greater than 5 g/cm^3 and are usually present as trace elements. From an environmental perspective, the heavy metals of most concern are toxic heavy metals such as mercury (Hg), lead (Pb), cadmium (Cd), chromium (Cr), cobalt (Co), nickel (Ni), and copper (Cu) [6]. Excessive lead ion content can affect children's intelligence, including their speaking ability, memory, and concentration. The safe limit for lead ions in drinking water is 100 µg/L, with the highest acceptable level being 50 µg/L [7,8]. The European Union classifies and regulates cadmium ions as highly hazardous toxic substances and carcinogens, limits

the amount of cadmium discharge into lakes, rivers, dumps, and farmland, and prohibits pesticides that contain cadmium ions. The allowable concentration of cadmium ions in drinking water is 10 ppb, and that in food coloring must be less than 15 ppm [9,10]. These heavy metals are discharged into the environment in many forms, of which ionic heavy metal pollution in water is the most common [11]. Even when the concentration of heavy metal ions in water may be low, heavy metals accumulate in the human environment and cause various diseases and disorders [12].

The main treatment methods for wastewater with heavy metal contamination are ion exchange [13], adsorption [14], chemical precipitation [15], redox methods [16], solvent extraction [17], and membrane filtration (such as electrodialysis, nanofiltration, reverse osmosis, microfiltration, and ultrafiltration) [18]. Adsorption has the advantages of simplicity, high efficiency, low energy consumption, and renewability [19,20]. Adsorption is widely used for the recovery of heavy metals in sewage treatment [7,8]. Traditional adsorbent materials are usually made from acrylic acid, acrylamide, or their derivatives by chemical crosslinking polymerization [21]. Traditional adsorbent materials have relatively low specific surface areas and adsorption rates and cannot be easily recycled many times, all of which limit their application in practice [22].

Various adsorption materials, such as silica gel, activated carbon, resins, metal–organic frameworks, clays, and polymers have been used extensively to remove various pollutants from water bodies [23,24]. Membranes based on natural biopolymers are used in applications such as microfiltration, ultrafiltration, reverse osmosis, and nanofiltration membrane processes because of their low cost, availability, biodegradability, and natural origin [4]. The adsorbent chitosan is used extensively to treat water that has been polluted by harmful metal ions, antibiotic residues, and other pollutants, because of its high content of hydroxyl and amino functional groups and its biocompatibility, low toxicity, and biodegradability [25–27]. Chitosan has several shortcomings that limit its practical application: mechanical instability, sensitivity to pH, a challenging separation and recovery process, and low equilibrium capacity [28]. Several different modification methods have been studied to overcome these limiting factors [29,30]. The stability of chitosan in acidic solutions is increased by modifying it using crosslinking agents such as glyoxal, glutaraldehyde, and ethylenediamine, which usually act on the -NH_2 or -OH of chitosan to change its chemical properties. Cross-linking can also improve the pore size distribution and adsorption/desorption performance [31].

To improve the mechanical and chemical properties of chitosan, polyvinyl alcohol (PVA) has been mixed with chitosan to form hydrogen bonds [32]. As a result, the hydrophobic side chains of the blend can be aggregated, and the intermolecular and intramolecular hydrogen bonds can interact [33]. Composites of chitosan and PVA have high adsorption capacity and are promising candidates for a broad range of applications in material development and wastewater treatment [34].

Chitosan and its derivatives are often prepared as gels, films, particles, and powders in practical applications [35]. Particulates are the most widely used form of adsorbent because their high specific surface areas result in excellent adsorption capacities [36]. However, the separation and recovery of heavy metals from particulate adsorbents are complex, cost-intensive, and time-consuming [37]. Magnetic separation technology can effectively separate magnetic materials from aqueous solutions and has the advantages of low operating cost, fast separation speed, and large processing capacity [38,39]. Magnetite (Fe_3O_4) is widely used as a magnetic material blend with chitosan because of its chemical stability, biocompatibility, favorable magnetic properties, and large surface area [25]. However, because of the van der Waals force between the nano-Fe_3O_4 particles and the magnetic force, accumulation is prone to occur. This reduces the specific surface area of the magnetic hydrogel, which reduces its ability to adsorb heavy metals [40].

Mesoporous SiO_2 is widely used in adsorption and separation because of its uniform pore structure, large specific surface area, and good pore size characteristics [41]. Wrapping SiO_2 in the outer layer of nano-Fe_3O_4 can effectively slow down the accumulation of

nano-Fe_3O_4 and improve the adsorption capacity of magnetic mesoporous microspheres for heavy metals [42]. To further enhance the adsorption capacity of chitosan, various modifications with new functional groups such as ethylenediamine, thiourea, isatin, and xanthate have been extensively studied [43]. The modification of chitosan with xanthate can improve the interaction between chitosan and heavy metals in solution, thereby increasing the adsorption capacity [44].

In this work, a novel magnetic xanthate-modified adsorbent was designed and synthesized by surface modification of Fe_3O_4@SiO_2/PVA/CS (XMPC) with the aim of improving the properties of chitosan, including its adsorption capacity, reusability, and mechanical stability. The synthesized XMPC adsorbents were characterized, and their adsorption properties for the removal of Pb(II), Cd(II), and Cu(II) from aqueous solutions under different experimental conditions were studied. Additionally, the adsorption/desorption performance of XMPC was also evaluated in batch experiments.

2. Experimental Method

2.1. Materials

Chitosan and PVA-1788 were from Sinopharm Chemical Reagent Co., Ltd. (Shanghai, China). Other reagents and chemicals were from Sigma Aldrich (St. Louis, MO, USA), Acros Organics (Geel, Belgium), and Fisher Scientific (Hampton, NH, USA), unless otherwise noted, and were used without further purification. All other chemicals were commercially available analytical-grade reagents. All solutions were prepared with deionized water.

2.2. Preparation of XMPC

Magnetic CS/PVA was prepared by a momentary gelation method. The chitosan–acetate solution was prepared by the dissolution of chitosan powder (6 g) in 150 mL of 2% (*v/v*) aqueous acetic acid at room temperature, and the PVA solution was prepared by the dissolution of 6 g of PVA powder in 150 mL of deionized water that was added to the chitosan–acetate solution. Fe_3O_4@SiO_2 (1.2 g) was added into the mixture. The composite gel-forming solution was stirred continuously for 3 h at 30 °C until the Fe_3O_4@SiO_2/PVA/CS (MPC) solution became a homogeneous magnetic gel solution. The gel-forming solution was dropped slowly into 1.0 M sodium hydroxide (NaOH), which resulted in the immediate formation of spherical hydrogel beads. The beads were gelled for 1 h and washed ten times with deionized water. Wet beads were dipped into glutaraldehyde solution (0.046 mL, 0.12 mmol) and stirred for 12 h at 30 °C to obtain crosslinked magnetic CS/PVA. After thorough washing with deionized water, the crosslinked magnetic PVA/CS beads were filtered and dried at 70 °C for 24 h. The PVA/CS beads (2 g) were treated with 100 mL of 14% NaOH solution and 1 mL of carbon disulfide (CS_2). The mixture was stirred at room temperature for 24 h. The product was washed thoroughly with distilled water and dried at 70 °C for 24 h.

2.3. Analytical Methods

Fourier transform infrared spectroscopy (FTIR) measurements were performed on a Nicolet 6700 spectrometer equipped with an MCT detector. Thermogravimetric analysis (TGA) was undertaken with a NETZSCH STA 449C instrument, and measurements were performed from 25 °C to 700 °C, at a heating rate of 20 °C/min in N_2. Differential scanning calorimetry (DSC) was performed on a NETZSCH DSC 200 PC unit from –50 °C to 300 °C, at a heating rate of 10 °C/min in N_2. Raman spectra were obtained with a laser confocal microscope spectrometer (American Thermoelectric Corporation). The surface morphologies of the XMPC were visualized by SEM (SSX-550, Shimadzu, Kyoto, Japan). An X-ray diffraction (XRD) study of the samples was carried out on a Bruker D8 Focus +X-ray diffractometer operating at 30 kV and 20 mA with a copper target (l = 1.54 Å) and at a scanning rate of 1° min^{-1}. The surface areas were determined by Brunauer–Emmett–Teller (BET) analysis (AUTOSORBiQ2, Quantachrome, Boynton Beach, FL, USA). Metal ion

concentrations were determined by atomic absorption spectroscopy (SSX-550, Shimadzu, Kyoto, Japan).

3. Results and Discussion

3.1. Preparation and Characterization

The procedure used to synthesize the XMPC is illustrated in Scheme 1. First, chitosan and PVA were dissolved in an acetic acid solution, in which the PVA had good dispersion stabilization. Fe_3O_4@SiO_2 was then added such that it dispersed evenly, and the MPC was prepared by crosslinking with glutaraldehyde. The MPC was modified by reaction with CS_2 under alkaline conditions to obtain the xanthate-modified adsorbent XMPC.

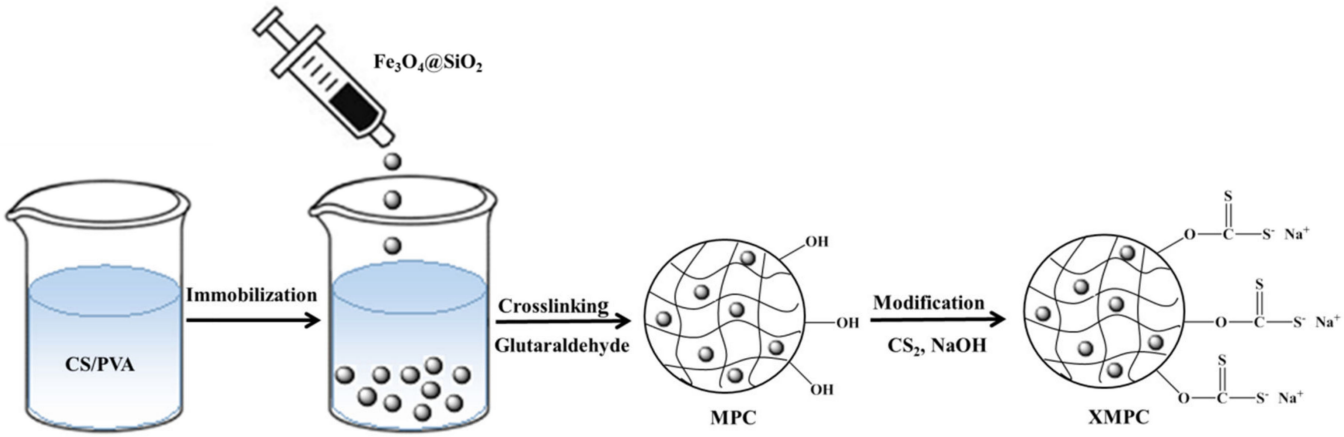

Scheme 1. The procedure for the preparation of the MPC and XMPC.

The infrared spectra of unmodified magnetic PVA/CS (MPC) and xanthate-modified magnetic PVA/CS (XMPC) in the range of 500–4000 cm^{-1} are shown in Figure 1a. The primary characteristic bands were as follows: in-plane bending vibration of O–H corresponding to the peak at 1400 cm^{-1}, stretching vibration of C–O–C corresponding to the peak at 1162 cm^{-1}, and absorption peaks at 3415 cm^{-1} and 581 cm^{-1} caused by the stretching of Fe–O bonds, indicating the presence of Fe_3O_4 in magnetic chitosan [30]. The absorption peaks at 1110 cm^{-1} were caused by the Si–O–Si vibrations, which also confirmed the formation of silicon shells on the surface of the Fe_3O_4 [45–48]. After the modification, the intensity of the characteristic peaks weakened, and the peak characteristics of C=S and S–C–S appeared at 1214 cm^{-1}, indicating the successful production of the thiol-based modified chitosan hydrogel [49,50]. The infrared spectrum of the XMPC indicated the presence of chitosan and Fe_3O_4@SiO_2. However, the peak indicating carbon disulfide modification was not pronounced, and the results of further analysis by Raman spectroscopy are shown in Figure 1b. The Raman spectrum of the MPC had two prominent peaks near 1345 cm^{-1} (D peak) and 1549 cm^{-1} (G peak). The peak at 1345 cm^{-1} was the bending vibration peak of NH, and the peak at 1549 cm^{-1} was the stretching vibration peak of C=C. After modification with xanthate, the D peak and G peak of the XMPC were weaker, and a peak characteristic of the C–S single bond appeared at 2908 cm^{-1}, indicating the success of xanthate modification. Based on the comparison with the peak data of the Joint Committee on Powder Diffraction Standards file, the diffraction patterns for Fe_3O_4 and SiO_2 (Figure 1c) were found to have broad peaks at 30.17°, 35.08°, 43.00°, 56.92°, and 62.45°, corresponding to (2 2 0), (3 1 1), (4 0 0), (5 1 1), and (4 4 0), respectively [51]. The diffraction intensity of the prepared XMPC decreased, indicating a decline in crystallinity. This decline was due to intramolecular hydrogen bonding with the polymer and the intermolecular hydrogen bonding interaction of the amino and hydroxyl groups to chitosan and PVA, respectively. This result indicated that Fe_3O_4@SiO_2 nanoparticles were successfully introduced into the PVA/CS material.

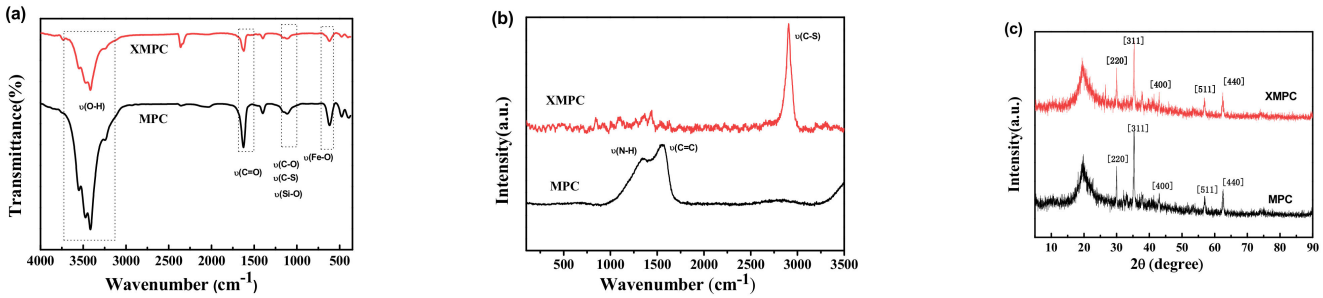

Figure 1. (**a**) FTIR spectra, (**b**) Raman spectra, and (**c**) XRD patterns of the XMPC and MPC.

The thermal characteristics of the XMPC were determined by its thermogravimetric analysis (TG) and differential scanning calorimeter (DSC) curves, and the results are shown in Figure 2a,b. In the TG and DTG curves, slight weight loss occurred below 150 °C, corresponding to the evaporation of absorbed and linked water in the material. The most significant weight loss occurred between 150 °C and 450 °C as a result of the structural degradation of CS and PVA. The final weight loss between 450 °C and 750 °C was attributed to charring due to the temperature exceeding the maximum degradation temperature of the material [52]. In the DSC curve, shown in Figure 2b, an exothermic peak was observed at approximately 101.2 °C, which may be due to the release of bound water in the XMPC. This was supported by the results of TGA. The glass transition temperatures (Tg) of PVA and CS were not found in the DSC curve, which also indicated that the new material, the XMPC, was formed successfully.

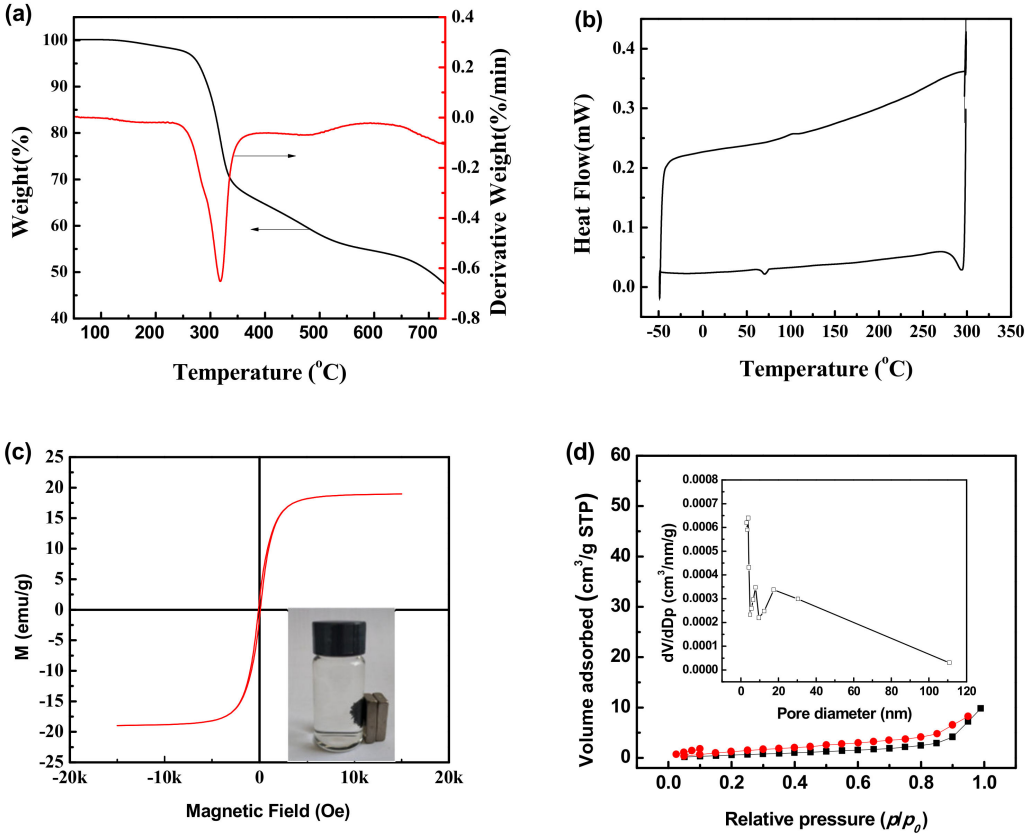

Figure 2. (**a**) TG and (**b**) DSC curves of the XMPC; (**c**) magnetization curves of the XMMCP; (**d**) N_2 adsorption–desorption isotherm of the XMPC. Inset: BJH pore size distribution of the XMPC.

The magnetization curve of the hydrogel XMPC and its magnetic responsive behavior are shown in Figure 2c. The magnetic hysteresis loop with an S-like shape was symmetrical about the origin without hysteresis, remanence, or coercivity, implying that the material was superparamagnetic. The saturation magnetization of the XMPC was 18.79 emu/g, which is sufficient for magnetic separation in a solution. As the inset of Figure 2c shows, when a magnet was placed close to the glass bottle, the adsorbent material quickly gathered on the side of the glass bottle close to the magnet, indicating that the adsorbent material had favorable magnetic response characteristics [53].

Figure 2d shows the N_2 adsorption–desorption isotherm of the XMPC, and the inset shows its Barrett–Joyner–Halenda (BJH) pore size distribution. The Brunauer–Emmett–Teller (BET) isotherm of the XMPC was characteristic of type IV adsorption–desorption behavior. When the relative pressure (P/P_0) was within the range of 0.70 to 0.95, the desorption isotherm exhibited hysteresis typical of a mesoporous structure. The specific surface area of the material calculated from the N_2 adsorption–desorption isotherm using the BET equation was found to be 3.65 m^2/g, and the total pore volume was found to be 0.016 cm^3/g. The BJH pore size distribution of the XMPC was between 0.5 nm and 5 nm and was mainly concentrated in a single peak. These results indicated that the material had a low specific surface area [54]. The microstructures of the XMPC and MPC were characterized by SEM (Figure 3). Their morphologies were similar, and the modified surface chemical groups did not change their original morphologies. The XMPC had a loose structure with interconnected pores, which enhanced the adsorption capacity, providing more adsorption sites on the surface and inside the adsorbent.

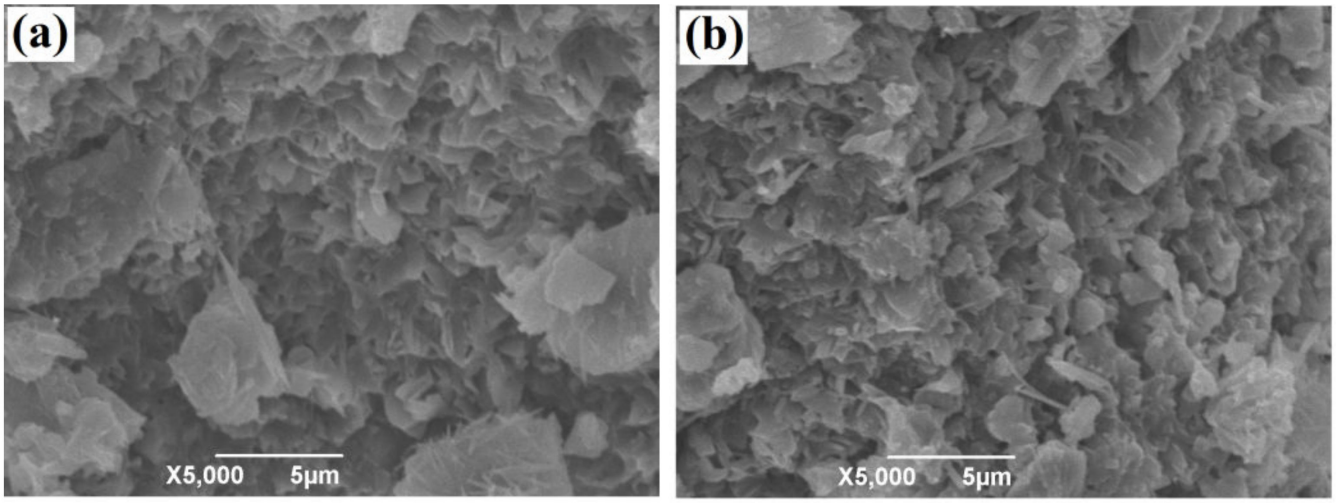

Figure 3. SEM images of (**a**) the MPC and (**b**) XMPC.

The XMPC was tested in deionized water and acidic and primary media for 10 d; the related data are shown in Table S1. There was no significant change in mass after 10 d (<1.0%). This may be due to the crosslinking of glutaraldehyde and the hydrogen bond interactions of PVA, CS, and Fe_3O_4@SiO_2. This indicated that the modified material had enhanced durability in acidic and primary environments.

3.2. Evaluation of Adsorption and Desorption Performance

The adsorption uptake of heavy metal ions in water by the magnetic composite is shown as a function of time in Figure 4. The XMPC had a good adsorption effect on heavy metal ions in wastewater and is thus an excellent choice for treating wastewater. In the initial stage of adsorption, because of the higher concentration of the heavy metal ion solution, there were more adsorption groups on the hydrogel, and the adsorption rate of the heavy metal ions by the hydrogel was also faster. However, as contact time increased, the adsorption groups on the hydrogel were gradually filled with heavy metal ions, and the

forces between the heavy metal ions on the hydrogel and the heavy metal ions in the water became stronger. After approximately 2 h, the adsorption capacity reached saturation, and the adsorption process became stable. The adsorption capacities of the XMPC for Cu(II), Pb(II), and Cd(II) ions were 67 mg/g, 100 mg/g, and 307 mg/g, respectively. The adsorption capacities of MPC for the Cu(II), Pb(II), and Cd(II) ions under the same conditions were 51 mg/g, 82 mg/g, and 220 mg/g, respectively. Chitosan modification with xanthate resulted in an improved interaction between the chitosan and heavy metals in solution, which increased the adsorption capacity. Related adsorbents were compared with the current adsorbent (XMPC), and the results are summarized in Table 1.

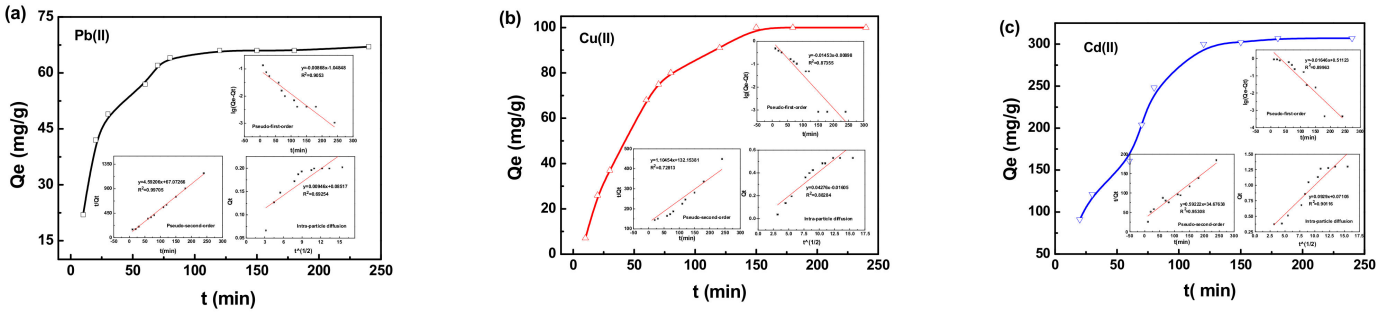

Figure 4. Effect of contact time on the adsorption capacity of the XMPC composite particles (303 K 1 g/L, pH = 5.5); adsorption of Pb(II) (**a**), Cu(II) (**b**), and Cd(II) (**c**). Insets: pseudo-first-order kinetic model, pseudo-second-order kinetic model, and intra-particle diffusion model.

To understand the adsorption process, the experimental data were modeled using pseudo-first-order, pseudo-second-order kinetic, and intra-particle diffusion models [55–57]. The fit equations are shown in the Supplementary Material. Table 2 shows that quasi-first-order kinetics cannot accurately describe the mechanism of adsorption of heavy metal ions in solution by the composite material. There was a strong linear relationship between t/Qt and t. The quasi-second-order kinetic equation more accurately described the adsorption mechanism of the hydrogel, indicating that the process of the adsorption of heavy metal ions by the composite material was chemical adsorption. At the beginning of the adsorption process, there were many vacancies on the surface of the hydrogel that could be occupied by heavy metal ions. As the adsorption time increased, these vacancies on the hydrogel were gradually occupied. A concentration difference developed between the surface and interior of the hydrogel, leading to further adsorption of heavy metal ions, with the adsorption rate being affected by the intra-particle diffusion rate. Based on the above results, a mechanism for Cd(II) removal was proposed, as shown in Figure 5.

The influence of temperature on the adsorption capacity of Pb(II) Cu(II), and Cd(II) ions by the XMPC was studied at 293 K, 303 K, and 313 K (Figure 6). The adsorption isotherms were fit using the Langmuir and Freundlich models (Figure S1) [71,72]. The fitting equations are provided in the Supplementary Material. The standard Gibbs free energy change (ΔG°), standard enthalpy change (ΔH°), and standard entropy change (ΔS°) as functions of temperature were determined using the equations in the Supplementary Material. The calculated thermodynamic parameters are presented in Tables 3 and 4.

Table 1. Various chitosan-based adsorbents designed for removing of Cu(II), Pb(II), and Cd(II) ions from aqueous solutions.

Adsorbent	Qm (mg/g)			Conditions		Ref.
	Cu(II)	Pd(II)	Cd(II)	pH	T (°C)	
Zeolite X/CS hybrid microspheres	152	-	-	5.5	25	[2]
CS/PVA/PEI membrane	86.08	-	112.13	6	25	[9]
Cobalt ferrite@SiO 2–CS/EDTA composite	-	-	127.79	6	25	[10]
Amidoxime-functionalized CS	190.7	-	-	5	25	[12]
CNTs–CHO–CS composite	115.84	-	-	7	25	[14]
CS–g–MA composite	312.4	-	-	6	25	[16]
Magnetic Bentonite/carboxymethyl CS/SA hydrogel beads	56.79	-	-	5	30	[20]
CS-VMT composite	-	166.67	55.48	4	30	[25]
MMT/CS	17.2	-	-	9	45	[27]
CS@NZVI	-	-	142.8	7	25	[28]
Crosslinked carboxylated CS/carboxylated nanocellulose hydrogel beads	-	334.9	-	4	35	[29]
Alginate/melamine/CS aerogel	-	1331.6	-	5.5	25	[30]
PEI-grafted magnetic CS microspheres	-	134.9	-	-	-	[31]
Polydopamine modified CS aerogels	-	441.2	-	5	45	[44]
Magnetic–CS–PAA nanocomposite	-	204.9	-	6	35	[53]
CS–pectin gel beads	169.4	266.5	177.64	4–9	50	[58]
Hydroxyapatite/CS composites	-	132.1	81.1	6	25	[59]
CS–PVA nanofibers	-	266.12	148.79	6, 8	25	[60]
MnO2/CS nanoparticles	-	126.1	-	4	50	[61]
Sodium tripolyphosphate crosslinked CS beads	-	-	99.8	7	55	[62]
Vermiculite blended CS	-	-	169	5.5	30	[63]
Thiourea-modified magnetic ion-imprinted CS/TiO2	-	-	256.41	7	25	[64]
Silica/CS composite	870	316	-	5	30	[65]
CS/PVA/PEI membrane	86.08	-	112.13	6	25	[66]
CS–g–PAA/APT	303.03	-	-	5.5	30	[67]
CS–MMT hydrogel	132.74	-	-	5	20	[68]
CS/TEOS/APTES nanofiber	640.5	575.5	-	6, 5.5	45	[69]
TEPA/CS/CoFe2O4 composite	168.067	228.311	-	5	30	[70]
XMPC	100	67	307	5.5	30	This work

Table 2. Dynamic parameters for the adsorption of metal ions on the XMPC.

	Pseudo-First-Order		Pseudo-Second-Order		Intra-Particle Diffusion	
Metal Ions	**K_1 (min^{-1})**	**R^2**	**K_2 (mg/g min)**	**R^2**	**K_i (mg/g $min^{1/2}$)**	**R^2**
Pb(II)	0.0087	0.9053	4.5921	0.9971	0.0095	0.6925
Cu(II)	0.0165	0.8996	0.5922	0.9531	0.0929	0.9012
Cd(II)	0.0145	0.8736	1.1045	0.7281	0.0428	0.8828

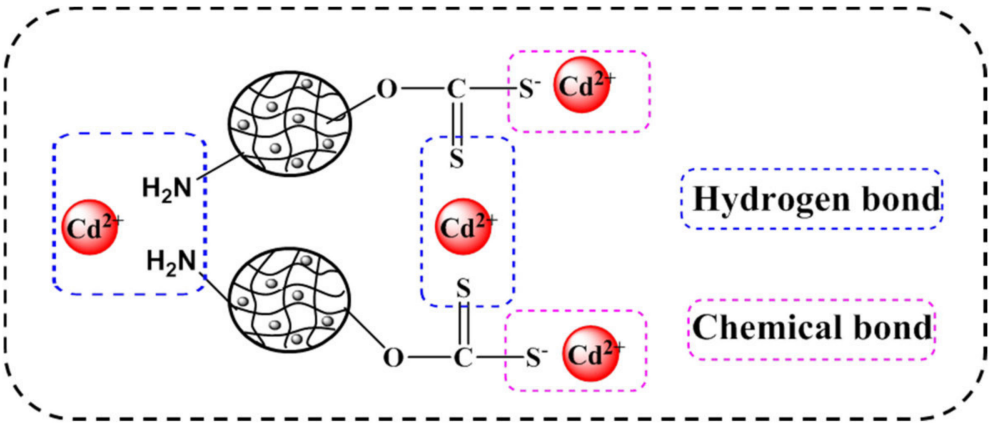

Figure 5. Proposed adsorption mechanism using the XMPC capture of Cd(II).

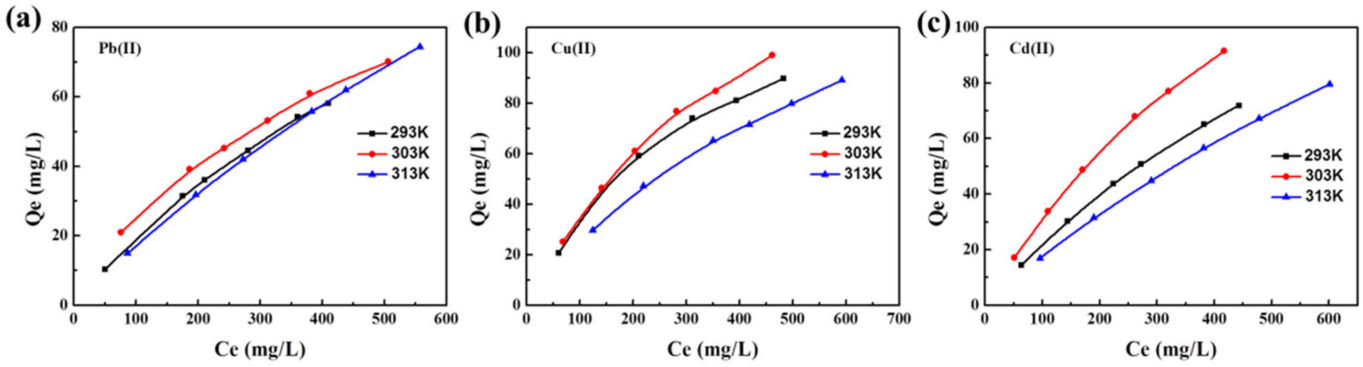

Figure 6. Effect of temperature on the adsorption of Pb(II) (**a**), Cu(II) (**b**), and Cd(II) (**c**) (pH = 5.5).

Table 3. Adsorption kinetics results for metal ions on the XMPC.

Metal Ions	T (K)	Langmuir			Freundlich		
		Q_m (mg/g)	K_L (L/mg)	R^2	K_F	b_F	R^2
Pb(II)	293 K	167.4743	0.001310	0.9960	0.4079	0.8322	0.9221
	303 K	188.5575	0.001742	0.9905	0.8813	0.7483	0.9873
	313 K	272.3575	0.000674	0.9997	0.3281	0.8623	0.9958
Cu(II)	293 K	161.6496	0.002636	0.9821	1.3139	0.6966	0.9703
	303 K	198.2883	0.002166	0.9931	1.2758	0.7186	0.9874
	313 K	183.9165	0.001560	0.9958	1.0658	0.6971	0.9936
Cd(II)	293 K	211.2975	0.001165	0.9996	0.4907	0.8241	0.9971
	303 K	234.0225	0.001546	0.9982	0.7557	0.8033	0.9953
	313 K	269.0434	0.000698	0.9982	0.3642	0.8463	0.9981

Table 4. Thermodynamic parameters for the adsorption of metal ions on the XMPC.

Metal Ions	T (K)	K_0	ΔG ($KJ \cdot mol^{-1}$)	ΔH ($KJ \cdot mol^{-1}$)	Δ S ($J \cdot mol^{-1} \cdot k^{-1}$)
Pb(II)	293	6.4412	−4.5376	6.5584	39.2971
	303	11.9197	−6.0369		
	313	7.5612	−4.9281		
Cu(II)	293	13.4735	−6.3354	1.1285	17.9890
	303	14.3811	−6.4942		
	313	13.0571	−6.2589		
Cd(II)	293	8.2486	−5.1401	0.4406	19.7548
	303	10.7766	−5.7913		
	313	8.2961	−5.1541		

As the concentration of metal ions increased, the adsorption groups of the composite material more fully contacted the ions, thereby increasing the adsorption capacity. This indicated that the concentration of the heavy metal ion solution strongly affected the adsorption capacity of the hydrogel. Figure 6 shows that adsorption by the composite material increased with the increase in temperature, which may occur because the increased temperature promoted irregular movement of the hydrogel and heavy metal ions. When the temperature exceeded 313 K, the adsorption capacity decreased slightly.

Figure S1 shows that the correlation coefficient for the Freundlich model was higher than that of the Langmuir model, which suggests that the adsorption process was bilayer adsorption. Larger values of K_0 indicated a faster adsorption rate. As the temperature increased, the adsorption rate gradually increased until the temperature reached 313 K. At this temperature, the high speed of molecular motion inhibited adsorption by the magnetic chitosan hydrogel. The chemical reaction process by which the hydrogel adsorbs heavy metal ions was spontaneous. The heat of chemical reaction in the adsorption process was 6.56 KJ/mol for Pb^{2+}, 1.23 KJ/mol for Cu^{2+}, and 0.44 KJ/mol for Cd^{2+}. The value of $\triangle$H was positive, indicating that the adsorption process was an endothermic reaction, so increasing the temperature would increase the adsorption rate [73,74]. If $\triangle$S is negative, it means that the system's entropy is reduced, which means that the hydrogel has absorbed the heavy metal ions in the water. This reduces the number of molecules that move randomly in the water.

3.3. Selective Adsorption Behaviors of Heavy Metals

The coexistence of multiple ions was studied at a temperature of 293 K and an adsorption time of 120 min. The adsorption performance and mutual influence of the XMPC on various heavy metal ions is shown in Table 5. In the single-component adsorption system, the modified composite material had better adsorption performance for heavy metal ions, especially Cd(II), with an adsorption capacity of 300 mg/g. In the multi-component system, that is when two or five ions compete for adsorption sites, the adsorption capacity for various ions was significantly reduced, especially in the mixed solution of five ions. Compared with the adsorption capacity of Cd(II) in the single-component system, the adsorption capacity was reduced by 80%. A larger distribution coefficient of the heavy metal ions in the multi-component system indicated that the ions had stronger affinity. The affinity of Cd(II) was strongest, as was the competitiveness of the active sites on the magnetic hydrogel. The smaller the value of the selectivity coefficient, the better the selectivity of the magnetic hydrogel for the measured ion was. The number of adsorption sites on the modified magnetic chitosan composite hydrogel was limited could overlap easily with the active sites on the hydrogel. When the hydrogel preferentially adsorbed the most

competitive Cd(II), the number of active sites occupied by other ions decreased, leading to different decreases in adsorption capacity for each different type of heavy metal ion. This experiment showed that during competitive adsorption, the affinity and selective adsorption of Cd(II) were both optimal.

Table 5. Selective adsorption by the XMPC from a solution of mixed components.

Metal Ions	Q_e (mg/g)	Kd	Ks
Pb(II)	66.34	-	-
Cu(II)	91.22	-	-
Co(II)	84.14	-	-
Ni(II)	21.21	-	-
Cd(II)	300.01	-	-
Cd(II) in mixed Cd(II)/Cu(II))	120.05	255.4	2.45
Cu(II) in mixed Cd(II)/Cu(II))	50.71	104.1	-
Cd(II) in mixed Cd(II)/Co(II))	118.79	252.6	1.92
Co(II) in mixed Cd(II)/Co(II))	63.72	131.6	-
Cd(II) in mixed Cd(II)/Ni(II))	156.19	338.8	9.67
Ni(II) in mixed Cd(II)/Ni(II))	17.36	35.0	-
Cd(II) in mixed (Pb(II)/Cd(II))	118.79	252.6	5.37
Pb(II) in mixed (Pb(II)/Cd(II))	23.25	47.0	-
Pb(II) in five mixed ions	20.44	41.3	-
Cu(II) in five mixed ions	37.01	75.4	-
Co(II) in five mixed ions	32.58	66.2	-
Ni(II) in five mixed ions	10.11	20.3	-
Cd(II) in five mixed ions	95.43	200.4	-

3.4. Desorption and Regeneration

Desorption is essential to enable the reuse of the adsorbent and recover metal ions. Desorption measurements were also used to elucidate the adsorption process. The exhausted adsorbent was eluted using HCl (pH = 1). Nine consecutive re-adsorption/desorption cycles to evaluate the adsorption efficiency of metal ions on the XMPC were conducted under the same conditions, and the results are shown in Figure 7 and Table S2. When the magnetic hydrogel adsorbed three heavy metal ions for the fourth time, the adsorption capacity was significantly reduced. As the magnetic hydrogel adsorption times increased, the ion adsorption capacity of the hydrogel decreased significantly. The curve in Figure 7c shows that the removal rate decreased as the number of cycles increased. Hydrochloric acid may destroy the structure of the magnetic hydrogel, thus causing the desorption rate to drop abruptly, and thereby affecting the overall adsorption performance of the magnetic hydrogel. After five cycles of adsorption and desorption, the adsorption capacity was still higher than 50%, which showed that the thiol-modified magnetic hydrogel could be regenerated and reused after desorption.

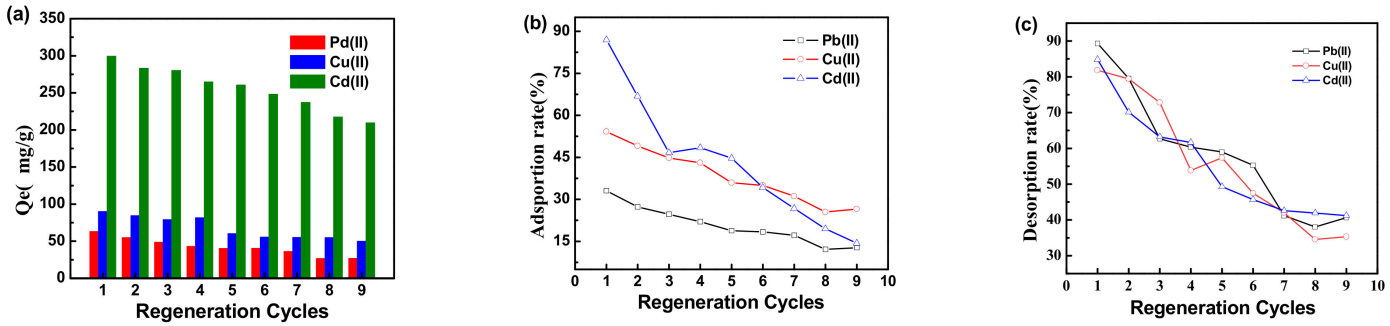

Figure 7. Adsorption capacity of the XMPC on metal ions during regeneration cycles, (**a**) adsorption capacity, (**b**) adsorption rate, and (**c**) desorption rate in regeneration cycles.

4. Conclusions

Magnetic hydrogel beads of the XMPC were prepared, and their adsorption of Pd(II), Cu(II), and Cd(II) ions was studied experimentally. The XMPC reached adsorption equilibrium after adsorption for about 120 min at 303 K, and the removal rates of Pd(II), Cu(II), and Cd(II) ions were 67 mg/g, 100 mg/g, and 307 mg/g, respectively. The adsorption of metal ions by the XMPC was a spontaneous and endothermic process and was well described by the quasi-secondary kinetic model and the Langmuir adsorption isotherm. The adsorbent was stable below 150 °C and had good magnetic properties. The adsorbent was found to be stable in deionized water, acidic, and basic media for at least 10 d. After five cycles of use, the removal rate of metal ions by the magnetic hydrogel beads remained above 50%. The results of this study showed that XMPC has not only the adsorption capacity of CS for metal ions, but also the magnetic properties of Fe_3O_4 and demonstrated the ease and speed of solid–liquid separation after adsorption by the XMPC.

Supplementary Materials: The following supporting information can be downloaded at: https://www.mdpi.com/article/10.3390/polym14061107/s1. Figure S1: Adsorption isotherms for metal ions on the XMPC. Table S1: Swelling ratio of the XMPC. Table S2: Adsorption and desorption data of heavy metal ion adsorption by the XMPC. Adsorption and desorption experiments, swelling experiments, adsorption studies, adsorption kinetics, adsorption isotherms, absorption thermodynamics, and selective adsorption behaviors of heavy metals.

Author Contributions: Conceptualization, S.W. and L.D.; Methodology, Y.L., A.Y. and Y.Z.; Software, Q.Z.; Validation, Y.L., A.Y. and Y.Z.; Formal analysis, X.D. and H.S.; Investigation, S.W., P.S. and B.Y.; Resources, S.W. and L.D.; Data curation, S.W. and L.D.; Writing—original draft preparation, S.W. and L.D.; Writing—review and editing, S.W. and L.D.; Visualization, S.W. and L.D.; Supervision, S.W. and L.D. All authors have read and agreed to the published version of the manuscript.

Funding: This work was supported by the Natural Science Foundation of Jiangsu Province (Nos. BK20180178 and BK20190157).

Institutional Review Board Statement: Not applicable.

Informed Consent Statement: Not applicable.

Data Availability Statement: Not applicable.

Conflicts of Interest: The authors declare no competing financial interest.

References

1. Ge, F.; Li, M.M.; Ye, H.; Zhao, B.X. Effective removal of heavy metal ions Cd^{2+}, Zn^{2+}, Pb^{2+}, Cu^{2+} from aqueous solution by polymer-modified magnetic nanoparticles. *J. Hazard. Mater.* **2012**, *211–212*, 366–372. [CrossRef] [PubMed]
2. Căprărescu, S.; Modrogan, C.; Purcar, V.; Dăncilă, A.M.; Orbuleț, O.D. Study of polyvinyl alcohol-SiO_2 nanoparticles polymeric membrane in wastewater treatment containing zinc ions. *Polymers* **2021**, *13*, 1875. [CrossRef] [PubMed]
3. Omer, A.M.; Dey, R.; Eltaweil, A.S.; Abd El-Monaem, E.M.; Ziora, Z.M. Insights into recent advances of chitosan-based adsorbents for sustainable removal of heavy metals and anions. *Arab. J. Chem.* **2022**, *15*, 103543. [CrossRef]

4. Căprărescu, S.; Zgârian, R.G.; Tihan, G.T.; Purcar, V.; Eftimie, T.E.; Modrogan, C.; Chiriac, A.-L.; Nicolae, C.A. Biopolymeric membrane enriched with chitosan and silver for metallic ions removal. *Polymers* **2020**, *12*, 1792. [CrossRef]
5. Sandu, T.; Sârbu, A.; Damian, C.M.; Marin, A.; Vulpe, S.; Budinova, T.; Tsyntsarski, B.; Yardim, M.F.; Sirkecioglu, A. Preparation and characterization of membranes obtained from blends of acrylonitrile copolymers with poly(vinyl alcohol). *J. Appl. Polym. Sci.* **2014**, *131*, 41013. [CrossRef]
6. Sun, G.L.; Reynolds, E.E.; Belcher, A.M. Designing yeast as plant-like hyperaccumulators for heavy metals. *Nat. Commun.* **2019**, *10*, 5080. [CrossRef]
7. Lv, L.; Chen, N.; Feng, C.; Gao, Y.; Li, M. Xanthate-modified magnetic chitosan/poly (vinyl alcohol) adsorbent: Preparation, characterization, and performance of Pb(II) removal from aqueous solution. *J. Taiwan Inst. Chem. Eng.* **2017**, *78*, 485–492. [CrossRef]
8. World Health Organization (WHO). Guidelines for Drinking-Water Quality. In *Recomendations*, 3rd ed.; World Health Organization: Geneva, Switzerland, 2008; Volume 1, pp. 390–399.
9. Sahebjamee, N.; Soltanieh, M.; Mousavi, S.M.; Heydarinasab, A. Removal of Cu^{2+}, Cd^{2+} and Ni^{2+} ions from aqueous solution using a novel chitosan/polyvinyl alcohol adsorptive membrane. *Carbohydr. Polym.* **2019**, *210*, 264–273. [CrossRef]
10. Wang, Y.; Zhou, R.; Wang, C.; Zhou, G.; Hua, C.; Cao, Y.; Song, Z. Novel environmental-friendly nano-composite magnetic attapulgite functionalized by chitosan and EDTA for cadmium (II) removal. *J. Alloys Compd.* **2020**, *817*, 153286. [CrossRef]
11. Karrari, P.; Mehrpour, O.; Abdollahi, M. A systematic review on status of lead pollution and toxicity in Iran; Guidance for preventive measures. *Daru* **2012**, *20*, 2. [CrossRef]
12. He, Y.; Gou, S.; Zhou, L.; Tang, L.; Liu, T.; Liu, L.; Duan, M. Amidoxime-functionalized polyacrylamide-modified chitosan containing imidazoline groups for effective removal of Cu^{2+} and Ni^{2+}. *Carbohydr. Polym.* **2021**, *252*, 117160. [CrossRef]
13. Gode, F.; Pehlivan, E. Removal of chromium(III) from aqueous solutions using Lewatit S 100: The effect of pH, time, metal concentration and temperature. *J. Hazard. Mater.* **2006**, *136*, 330–337. [CrossRef]
14. Dou, J.; Gan, D.; Huang, Q.; Liu, M.; Chen, J.; Deng, F.; Zhu, X.; Wen, Y.; Zhang, X.; Wei, Y. Functionalization of carbon nanotubes with chitosan based on MALI multicomponent reaction for Cu^{2+} removal. *Int. J. Biol. Macromol.* **2019**, *136*, 476–485. [CrossRef]
15. Fu, F.; Wang, Q. Removal of heavy metal ions from wastewaters: A review. *J. Environ. Manag.* **2011**, *92*, 407–418. [CrossRef]
16. Ibrahim, A.G.; Saleh, A.S.; Elsharma, E.M.; Metwally, E.; Siyam, T. Chitosan-g-maleic acid for effective removal of copper and nickel ions from their solutions. *Int. J. Biol. Macromol.* **2019**, *121*, 1287–1294. [CrossRef]
17. Surgutskaia, N.S.; Martino, A.D.; Zednik, J.; Ozaltin, K.; Lovecká, L.; Bergerová, E.D.; Kimmer, D.; Svoboda, J.; Sedlarik, V. Efficient Cu^{2+}, Pb^{2+} and Ni^{2+} ion removal from wastewater using electrospun DTPA-modified chitosan/polyethylene oxide nanofibers. *Sep. Purif. Technol.* **2020**, *247*, 116914. [CrossRef]
18. Landaburu-Aguirre, J.; Pongracz, E.; Peramaki, P.; Keiski, R.L. Micellar-enhanced ultrafiltration for the removal of cadmium and zinc: Use of response surface methodology to improve understanding of process performance and optimisation. *J. Hazard. Mater.* **2010**, *180*, 524–534. [CrossRef]
19. Yang, Z.; Zhao, Z.; Yang, X.; Ren, Z. Xanthate modified magnetic activated carbon for efficient removal of cationic dyes and tetracycline hydrochloride from aqueous solutions. *Colloids Surf. A* **2021**, *615*, 126273. [CrossRef]
20. Zhang, H.; Omer, A.M.; Hu, Z.; Yang, L.Y.; Ji, C.; Ouyang, X.K. Fabrication of magnetic bentonite/carboxymethyl chitosan/sodium alginate hydrogel beads for Cu (II) adsorption. *Int. J. Biol. Macromol.* **2019**, *135*, 490–500. [CrossRef]
21. Zhao, R.; Wang, Y.; An, Y.; Yang, L.; Sun, Q.; Ma, J.; Zheng, H. Chitin-biocalcium as a novel superior composite for ciprofloxacin removal: Synergism of adsorption and flocculation. *J. Hazard. Mater.* **2022**, *423*, 126917. [CrossRef]
22. Wu, Y.; Jiang, J.; Sun, Q.; An, Y.; Zhao, R.; Zheng, H.; Li, H. Efficient removal of both positively and negatively charged colloidal contaminants using amphoteric starch-based flocculants synthesized by low-pressure UV initiation. *Sep. Purif. Technol.* **2022**, *282*, 120120. [CrossRef]
23. Eltaweil, A.S.; Omer, A.M.; El-Aqapa, H.G.; Gaber, N.M.; Attia, N.F.; El-Subruiti, G.M.; Mohy-Eldin, M.S.; Abd El-Monaem, E.M. Chitosan based adsorbents for the removal of phosphate and nitrate: A critical review. *Carbohydr. Polym.* **2021**, *274*, 118671. [CrossRef]
24. Saheed, I.O.; Oh, W.D.; Suah, F.B.M. Chitosan modifications for adsorption of pollutants—A review. *J. Hazard. Mater.* **2021**, *408*, 124889. [CrossRef]
25. Chen, L.; Wu, P.; Chen, M.; Lai, X.; Ahmed, Z.; Zhu, N.; Dang, Z.; Bi, Y.; Liu, T. Preparation and characterization of the eco-friendly chitosan/vermiculite biocomposite with excellent removal capacity for cadmium and lead. *Appl. Clay Sci.* **2018**, *159*, 74–82. [CrossRef]
26. Abd El-Monaem, E.M.; Eltaweil, A.S.; Elshishini, H.M.; Hosny, M.; Abou Alsoaud, M.M.; Attia, N.F.; El-Subruiti, G.M.; Omer, A.M. Sustainable adsorptive removal of antibiotic residues by chitosan composites: An insight into current developments and future recommendations. *Arab. J. Chem.* **2022**, *15*, 103743. [CrossRef]
27. Cho, D.W.; Jeon, B.H.; Chon, C.M.; Kim, Y.; Schwartz, F.W.; Lee, E.S.; Song, H. A novel chitosan/clay/magnetite composite for adsorption of Cu(II) and As(V). *Chem. Eng. J.* **2012**, *200–202*, 654–662. [CrossRef]
28. Ahmadi, M.; Foladivanda, M.; Jaafarzadeh, N.; Ramezani, Z.; Ramavandi, B.; Jorfi, S.; Kakavandi, B. Synthesis of chitosan zero-valent iron nanoparticles-supported for cadmium removal: Characterization, optimization and modeling approach. *J. Water Supply Res. Technol.* **2017**, *66*, 116–130. [CrossRef]

29. Xu, X.; Ouyang, X.K.; Yang, L.Y. Adsorption of Pb(II) from aqueous solutions using crosslinked carboxylated chitosan/carboxylated nanocellulose hydrogel beads. *J. Mol. Liq.* **2021**, *322*, 114523. [CrossRef]
30. Gao, C.; Wang, X.L.; An, Q.D.; Xiao, Z.Y.; Zhai, S.R. Synergistic preparation of modified alginate aerogel with melamine/chitosan for efficiently selective adsorption of lead ions. *Carbohydr. Polym.* **2021**, *256*, 117564. [CrossRef]
31. Sun, X.; Yang, L.; Xing, H.; Zhao, J.; Li, X.; Huang, Y.; Liu, H. Synthesis of polyethylenimine-functionalized poly(glycidyl methacrylate) magnetic microspheres and their excellent Cr(VI) ion removal properties. *Chem. Eng. J.* **2013**, *234*, 338–345. [CrossRef]
32. Xie, Y.; Ren, L.; Zhu, X.; Gou, X.; Chen, S. Physical and chemical treatments for removal of perchlorate from water—A review. *Process Saf. Environ.* **2018**, *116*, 180–198. [CrossRef]
33. Huang, Y.; Zheng, H.; Hu, X.; Wu, Y.; Tang, X.; He, Q.; Peng, S. Enhanced selective adsorption of lead(II) from complex wastewater by DTPA functionalized chitosan-coated magnetic silica nanoparticles based on anion-synergism. *J. Hazard. Mater.* **2022**, *422*, 126856. [CrossRef] [PubMed]
34. Pakdel, P.M.; Peighambardoust, S.J. Review on recent progress in chitosan-based hydrogels for wastewater treatment application. *Carbohyd. Polym.* **2018**, *201*, 264–279. [CrossRef] [PubMed]
35. Boominathan, T.; Sivaramakrishna, A. Recent Advances in the Synthesis, Properties, and Applications of Modified Chitosan Derivatives: Challenges and Opportunities. *Top. Curr. Chem.* **2021**, *379*, 19. [CrossRef]
36. Zhu, H.Y.; Jiang, R.; Xiao, L.; Zeng, G.M. Preparation, characterization, adsorption kinetics and thermodynamics of novel magnetic chitosan enwrapping nanosized γ-Fe_2O_3 and multi-walled carbon nanotubes with enhanced adsorption properties for methyl orange. *Bioresour. Technol.* **2010**, *101*, 5063–5069. [CrossRef]
37. Chen, W.; Zhang, F.; Tang, Q.; Du, B.; Ma, D.; Zhao, Z.; Fan, L.; Luo, H.; Zhao, Z.; Huang, X.; et al. Evaluating the performance of bridging-assembly chelating flocculant for heavy metals removal: Role of branched architectures. *Chemosphere* **2022**, *289*, 133260. [CrossRef]
38. Wu, F.C.; Tseng, R.L.; Juang, R.S. A review and experimental verification of using chitosan and its derivatives as adsorbents for selected heavy metals. *J. Environ. Manag.* **2010**, *91*, 798–806. [CrossRef]
39. Xie, Y.H.; Wu, Y.L.; Qin, Y.H.; Yi, Y.; Liu, Z.; Lv, L.; Xu, M. Evaluation of perchlorate removal from aqueous solution by cross-linked magnetic chitosan/poly (vinyl alcohol) particles. *J. Taiwan Inst. Chem. Eng.* **2016**, *65*, 295–303. [CrossRef]
40. Córdova, B.M.; Infantas, G.C.; Mayta, S.; Huamani-Palomino, R.G.; Kock, F.V.C.; Montes de Oca, J.; Valderrama, A.C. Xanthate-modified alginates for the removal of Pb(II) and Ni(II) from aqueous solutions: A brief analysis of alginate xanthation. *Int. J. Biol. Macromol.* **2021**, *179*, 557–566. [CrossRef]
41. Ngah, W.S.W.; Teong, L.C.; Hanafiah, M.A.K.M. Adsorption of dyes and heavy metal ions by chitosan composites: A review. *Carbohydr. Polym.* **2011**, *83*, 1446–1456. [CrossRef]
42. Caporale, A.G.; Punamiya, P.; Pigna, M.; Violante, A.; Sarkar, D. Effect of particle size of drinking-water treatment residuals on the sorption of arsenic in the presence of competing ions. *J. Hazard. Mater.* **2013**, *260*, 644–651. [CrossRef] [PubMed]
43. Ma, W.; Dai, J.; Dai, X.; Yan, Y. Preparation and characterization of chitosan/kaolin/Fe_3O_4 magnetic microspheres and their application for the removal of ciprofloxacin. *Adsorpt. Sci. Technol.* **2014**, *32*, 775–790. [CrossRef]
44. Guo, C.; Wang, Y.; Wang, F.; Wang, Y. Adsorption Performance of Amino Functionalized Magnetic Molecular Sieve Adsorbent for Effective Removal of Lead Ion from Aqueous Solution. *Nanomaterials* **2021**, *11*, 2353. [CrossRef] [PubMed]
45. Huang, Y.; Hu, C.; An, Y.; Xiong, Z.; Hu, X.; Zhang, G.; Zheng, H. Magnetic phosphorylated chitosan composite as a novel adsorbent for highly effective and selective capture of lead from aqueous solution. *J. Hazard. Mater.* **2021**, *405*, 124195. [CrossRef]
46. Chen, W.; Tang, Q.; Liu, Z.; Luo, F.; Liao, Y.; Zhao, S.; Zhang, K.; Cheng, L.; Ma, D. Fabricating a novel chitosan-based adsorbent with multifunctional synergistic effect for Cu(II) removal: Maleic anhydride as a connecting bridge. *Chem. Eng. Res. Des.* **2020**, *163*, 21–35. [CrossRef]
47. He, M.; Chen, Z.; Xu, C.; Chen, B.; Hu, B. Magnetic nanomaterials as sorbents for trace elements analysis in environmental and biological samples. *Talanta* **2021**, *230*, 122306. [CrossRef]
48. Zeng, H.; Wang, L.; Zhang, D.; Yan, P.; Nie, J.; Sharma, V.K.; Wang, C. Highly efficient and selective removal of mercury ions using hyperbranched polyethylenimine functionalized carboxymethyl chitosan composite adsorbent. *Chem. Eng. J.* **2019**, *358*, 253–263. [CrossRef]
49. Liu, Y.; Fan, H.; Wang, X.; Zhang, J.; Li, W.; Wang, R. Controllable synthesis of bifunctional corn stalk cellulose as a novel adsorbent for efficient removal of Cu^{2+} and Pb^{2+} from wastewater. *Carbohydr. Polym.* **2022**, *276*, 118763. [CrossRef]
50. Wang, Q.; Tian, Y.; Kong, L.; Zhang, J.; Zuo, W.; Li, Y.; Cai, G. A novel 3D superelastic polyethyleneimine functionalized chitosan aerogels for selective removal of Cr(VI) from aqueous solution: Performance and mechanisms. *Chem. Eng. J.* **2021**, *425*, 131722. [CrossRef]
51. Qiao, L.; Wang, S.; Wang, T.; Yu, S.; Guo, S.; Du, K. High-strength and low-swelling chitosan/cellulose microspheres as a high-efficiency adsorbent for dye removal. *Cellulose* **2021**, *28*, 9323–9333. [CrossRef]
52. Chen, Y.; Wang, J. Preparation and characterization of magnetic chitosan nanoparticles and its application for Cu(II) removal. *Chem. Eng. J.* **2011**, *168*, 286–292.
53. Hu, D.; Lian, Z.; Xian, H.; Jiang, R.; Wang, N.; Weng, Y.; Peng, X.; Wang, S.; Ouyang, X.K. Adsorption of Pb(II) from aqueous solution by polyacrylic acid grafted magnetic chitosan nanocomposite. *Int. J. Biol. Macromol.* **2020**, *154*, 1537–1547. [CrossRef]

54. Chen, Y.; Wang, J. The characteristics and mechanism of Co(II) removal from aqueous solution by a novel xanthate-modified magnetic chitosan. *Nucl. Eng. Des.* **2012**, *242*, 452–457. [CrossRef]
55. Chandrakala, H.N.; Ramaraj, B.; Lee, J.H. Polyvinyl alcohol/carbon coated zinc oxide nanocomposites: Electrical, optical, structural and morphological characteristics. *J. Alloys Compd.* **2013**, *580*, 392–400. [CrossRef]
56. Selim, M.S.; Seoudi, R.; Shabaka, A.A. Polymer based films embedded with high content of ZnSe nanoparticles. *Mater. Lett.* **2005**, *59*, 2650–2654. [CrossRef]
57. Sun, X.; Yang, L.; Li, Q.; Zhao, J.; Li, X.; Wang, X.; Liu, H. Amino-functionalized magnetic cellulose nanocomposite as adsorbent for removal of Cr(VI): Synthesis and adsorption studies. *Chem. Eng. J.* **2014**, *241*, 175–183. [CrossRef]
58. Hu, Y.; Liu, T.; Chen, N.; Feng, C. Changes in microbial community diversity, composition, and functions upon nitrate and Cr(VI) contaminated groundwater. *Chemosphere* **2022**, *288*, 132476. [CrossRef]
59. Park, S.; Gomez-Flores, A.; Chung, Y.S.; Kim, H. Removal of cadmium and lead from aqueous solution by hydroxyapatite/chitosan hybrid fibrous sorbent: Kinetics and equilibrium studies. *J. Chem.* **2015**, *2015*, 396290. [CrossRef]
60. Karim, M.R.; Aijaz, M.O.; Alharth, N.H.; Alharbi, H.F.; Al-Mubaddel, F.S.; Awual, M.R. Composite nanofibers membranes of poly(vinyl alcohol)/chitosan for selective lead(II) and cadmium(II) ions removal from wastewater. *Ecotoxicol. Environ. Saf.* **2019**, *169*, 479–486. [CrossRef]
61. Dinh, V.P.; Le, N.C.; Tuyen, L.A.; Hung, N.Q.; Nguyen, V.D.; Nguyen, N.T. Insight into adsorption mechanism of lead(II) from aqueous solution by chitosan loaded MnO_2 nanoparticles. *Mater. Chem. Phys.* **2018**, *207*, 294–302. [CrossRef]
62. Prakash, N.; Soundarrajan, M.; Arungalai Vendan, S.; Sudha, P.N.; Renganathan, N.G. Contemplating the feasibility of vermiculate blended chitosan for heavy metal removal from simulated industrial wastewater. *Appl. Water Sci.* **2017**, *7*, 4207–4218. [CrossRef]
63. Babakhani, A.; Sartaj, M. Removal of Cadmium (II) from aqueous solution using tripolyphosphate cross-linked chitosan. *J. Environ. Chem. Eng.* **2020**, *8*, 103842. [CrossRef]
64. Chen, A.; Zeng, G.; Chen, G.; Hu, X.; Yan, M.; Guan, S.; Shang, C.; Lu, L.; Zou, Z.; Xie, G. Novel thiourea-modified magnetic ion-imprinted chitosan/TiO2 composite for simultaneous removal of cadmium and 2,4-dichlorophenol. *Chem. Eng. J.* **2012**, *191*, 85–94. [CrossRef]
65. Li, Z.; Xiao, D.; Ge, Y.; Koehler, S. Surface-functionalized porous lignin for fast and efficient lead removal from aqueous solution. *ACS Appl. Mater. Interfaces* **2015**, *7*, 15000–15009. [CrossRef]
66. Rajiv Gandhi, M.; Meenakshi, S. Preparation and characterization of silica gel/chitosan composite for the removal of Cu(II) and Pb(II). *Int. J. Biol. Macromol.* **2012**, *50*, 650–657. [CrossRef]
67. Wang, X.; Zheng, Y.; Wang, A. Fast removal of copper ions from aqueous solution by chitosan-g-poly(acrylic acid)/attapulgite composites. *J. Hazard. Mater.* **2009**, *168*, 970–977. [CrossRef]
68. Ngwabebhoh, F.A.; Erdem, A.; Yildiz, U. Synergistic removal of Cu(II) and nitrazine yellow dye using an eco-friendly chitosan-montmorillonite hydrogel: Optimization by response surface methodology. *J. Appl. Polym. Sci.* **2016**, *133*, 43664. [CrossRef]
69. Sabourian, V.; Ebrahimi, A.; Naseri, F.; Irani, M.; Rahimi, A. Fabrication of chitosan/silica nanofibrous adsorbent functionalized with amine groups for the removal of Ni(ii), Cu(ii) and Pb(ii) from aqueous solutions: Batch and column studies. *RSC Adv.* **2016**, *6*, 40354–40365. [CrossRef]
70. Fan, C.; Li, K.; Li, J.; Ying, D.; Wang, Y.; Jia, J. Comparative and competitive adsorption of Pb(II) and Cu(II) using tetraethylenepentamine modified chitosan/$CoFe_2O_4$ particles. *J. Hazard. Mater.* **2017**, *326*, 211–220. [CrossRef]
71. Ren, Y.; Abbood, H.A.; He, F.; Peng, H.; Huang, K. Magnetic EDTA-modified chitosan/SiO_2/Fe_3O_4 adsorbent: Preparation, characterization, and application in heavy metal adsorption. *Chem. Eng. J.* **2013**, *226*, 300–311. [CrossRef]
72. Zhou, L.; Shang, C.; Liu, Z.; Huang, G.; Adesina, A.A. Selective adsorption of uranium(VI) from aqueous solutions using the ion-imprinted magnetic chitosan resins. *J. Colloids Interface Sci.* **2012**, *366*, 165–172. [CrossRef] [PubMed]
73. Xu, P.; Zheng, M.; Chen, N.; Wu, Z.; Xu, N.; Tang, J.; Teng, Z. Uniform magnetic chitosan microspheres with radially oriented channels by electrostatic droplets method for efficient removal of Acid Blue. *J. Taiwan Inst. Chem. Eng.* **2019**, *104*, 210–218. [CrossRef]
74. Shao, Z.; Lu, J.; Ding, J.; Fan, F.; Sun, X.; Li, P.; Fang, Y.; Hu, Q. Novel green chitosan-pectin gel beads for the removal of Cu(II), Cd(II), Hg(II) and Pb(II) from aqueous solution. *Int. J. Biol. Macromol.* **2021**, *176*, 217–225. [CrossRef] [PubMed]